EFFECT OF NEUTRON IRRADIATION ON COMMERCIALISED B₂O₃-SiO₃ GLASS SLIDE FOR RADIATION DOSIMETRY

MUHAMMAD FAHMI BIN MOHD ZAINAL

17163319/2

PHYSICS DEPARTMENT, FACULTY OF SCIENCE
UNIVERSITY OF MALAYA
KUALA LUMPUR

FINAL YEAR PROJECT
SESSION 2019/2020
SIF3004

MUHAMMAD FAHMI BIN MOHD ZAINAL
17163319/2

FINAL YEAR THESIS SUBMITTED IN FULFILMENT OF THE REQUIREMENTS FOR THE DEGREE OF SCIENCE IN PHYSICS

PHYSICS DEPARTMENT, FACULTY OF SCIENCE
UNIVERSITY OF MALAYA
KUALA LUMPUR

SESSION 2021 / 2022

UNIVERSITY OF MALAYA

ORIGINAL LITERARY WORK DECLARATION

Name of Candidate: MUHAMMAD FAHMI BIN MOHD ZAINAL

(I.C/Passport No: (000922-14-1417)

Matric No: 17163319/2

Name of Degree: BACHELOR OF SCIENCE (PHYSICS)

Title of Project Paper: EFFECT OF NEUTRON IRRADIATION ON COMMERCIALISED B_2O_3-SiO_3 GLASS SLIDE FOR RADIATION DOSIMETRY

Field of Study: Physics

I do solemnly and sincerely declare that:

(1) I am the sole author/writer of this Work;
(2) This Work is original;
(3) Any use of any work in which copyright exists was done by way of fair dealing and for permitted purposes and any excerpt or extract from, or reference to or reproduction of any copyright work has been disclosed expressly and sufficiently and the title of the Work and its authorship have been acknowledged in this Work;
(4) I do not have any actual knowledge nor do I ought reasonably to know that the making of this work constitutes an infringement of any copyright work;
(5) I hereby assign all and every rights in the copyright to this Work to the University of Malaya ("UM"), who henceforth shall be owner of the copyright in this Work and that any reproduction or use in any form or by any means whatsoever is prohibited without the written consent of UM having been first had and obtained;
(6) I am fully aware that if in the course of making this Work I have infringed any copyright whether intentionally or otherwise, I may be subject to legal action or any other action as may be determined by UM.

Candidate's Signature   Date: 25 JUNE 2022

Subscribed and solemnly declared before,

DR. SITI FAIRUS ABDUL SANI

Witness's Signature   Date: 25 JUNE 2022

Name:

Designation:

Dr. Siti Fairus Abdul Sani
Senior Lecturer
Department Of Physics,
Faculty Of Science,
University of Malaya.

ABSTRACT

In this present investigation, study has been made of thermoluminescence (TL) glow curve, dose response, sensitivity and linearity index of commercialise borosilicate glass slide. Herein, we have investigated the suitability of the samples for use as thermoluminescence detectors, to determine dose received by patients during radiation-based therapy, in this case for neutron irradiation. The samples were investigated by comparing the thermoluminescence response of the borosilicate glass slide of 1 mm thickness with different brands, e.g. silane and HmBg. Irradiation of neutron was undertaken at the TRIGA research reactor located at the Nuclear Agency Malaysia based on in-core neutron flux at 750 kW thermal powers. Doses ranging from 2 to 10 Gy were delivered with irradiation times within 30 s to 2.5 min. The TL response of the HmBg borosilicate glass slides showed linear with dose, resulting linear regression close to 0.97, while the Silane borosilicate glass slide gives the greatest TL response with regression factor of 0.66. In addition to the thermoluminescence study, characterisation using FTIR and Raman spectroscopy have been carried out to understand the defects (e.g. extrinsic or intrinsic) that give rise to the luminescence signal, allowing the Si-O-Si coordination to be identified and studied. The results show that borosilicate glass slide in the flat form demonstrate excellent characteristics for use as radiation sensors for measurement of the doses received by patients in clinical applications.

Keywords: Borosilicate glass slide, neutron irradiation, dosimetry, thermoluminescence, FTIR and Raman spectroscopy

ABSTRAK

Dalam penyiasatan ini, kajian telah dibuat tentang lengkung cahaya termoluminesen (TL), tindak balas dos, kepekaan kaca borosilikat dan indeks kelinearan bagi slaid kaca borosilikat yang dikomersialkan. Di sini, kami telah menyiasat kesesuaian sampel untuk digunakan sebagai pengesan termoluminesen, untuk menentukan dos yang diterima oleh pesakit semasa terapi berasaskan sinaran, dalam kes ini ,untuk penyinaran neutron. Sampel disiasat dengan membandingkan tindak balas termoluminesen bagi slaid kaca borosilikat dengan ketebalan 1 mm dengan jenama yang berbeza, cth. Silane dan HmBg. Penyinaran neutron telah dilakukan di reaktor penyelidikan TRIGA yang terletak di Agensi Nuklear Malaysia berdasarkan fluks neutron dalam teras pada kuasa haba 750 kW. Dos antara 2 hingga 10 Gy telah dihantar, masa penyinaran dalam 30 s hingga 2.5 min. Tindak balas TL bagi slaid kaca borosilikat HmBg menunjukkan linear dengan dos, menghasilkan regresi linear menghampiri 0.97, manakala slaid kaca borosilikat Silane memberikan tindak balas TL yang paling besar dengan faktor regresi 0.66. Sebagai tambahan kepada kajian termoluminesen, pencirian menggunakan spektroskopi FTIR dan spektroskopi Raman telah dijalankan untuk memahami kecacatan (contohnya ekstrinsik atau intrinsik) yang menimbulkan isyarat luminesen, membolehkan koordinasi Si-O-Si dikenal pasti dan dikaji. Keputusan menunjukkan bahawa slaid kaca borosilikat dalam bentuk rata menunjukkan ciri-ciri yang sangat baik untuk digunakan sebagai pengesan sinaran untuk pengukuran dos yang diterima oleh pesakit dalam aplikasi klinikal.

Kata kunci: Slaid kaca borosilikat, penyinaran neutron, dosimetri, termoluminesen, spectroskopi FTIR dan spektroskopi Raman.

ACKNOWLEDGEMENTS

TABLE OF CONTENTS

LIST OF FIGURES

LIST OF TABLES

CHAPTER 1: INTRODUCTION

1.1   Background

Radiotherapy is a cancer treatment that employs high doses of ionising radiation to destroy cancer cells and reduce tumours (Brundha et al., 2019). When radiation travels through a substance, ionisation occurs; this ionisation may be detrimental to the chemical structure of the substance. If the matter is biological, such as cells that create the organs and tissues of humans, and if critical chemical matter inside cells, such as the DNA molecule that forms a chromosome in the cell nucleus, is destroyed, the cells will be harmed. Moreover, ionising radiation has the potential to produce genetic abnormalities, which might pose issues for future generations. In order to decrease the amount of damage caused to nearby healthy cells, it is essential to monitor the dosage of radiation received.

It is vital to deliver radiation dosage particularly to a tumour in order to reduce the amount of radiation absorbed by the healthy cells and tissues in the proximity. In this situation, dosimetry is a crucial concept to study. During the process of radiation dose measurement, dosimeters are used in order to quantify the entry dose. In addition, thermoluminescence dosimeters, commonly known as TLDs, are often used in tissue-equivalent spectres to assess the delivery of alternative treatment methods. This eliminates the need for experts to utilise wires. Using borosilicate glass improves the accuracy of the previously described radiation dosimetry (Huston et al., 2001; Rivera, 2012a; Sani et al., 2021; Sani, Othman, et al., 2020) .Depending on the composition and temperature history of the glass, borosilicate glasses may demonstrate a high level of chemical complexity.It is well acknowledged that these glasses possess exceptional resistance to both thermal shock and chemical exposure (Smedskjaer et al., 2011).

Microscope glass slides has a number of desired characteristics, including the capacity to give a ready-made product that is mechanically durable in a range of thicknesses,

chemically inert, biocompatible, reusable, and simple to sterilise. When exposed to neutrons, photons, gamma rays, and x rays, borosilicate glass emits a considerable quantity of thermal luminosity (TL). This is due to the material's high number of intrinsic defects (Sani et al., 2021; Sani, Othman, et al., 2020). Therefore, this has prompted more research into the use of borosilicate glass slides as thermoluminescence dosimeters.

In present study, thermoluminescence characterisation on borosilicate glass slides irradiated to neutrons is investigated.

Neutrons interact with matter relatively weak and may thus penetrate it. In terms of the basic interaction mechanisms, their interactions are dissimilar from those of photons. Despite the fact that photons have no electrical charge, it is possible to interpret them as disturbances in the electromagnetic field; as a consequence, they may interact with electrons. Neutrons on the other hand, do not emit any electrical charge as no interaction through the Coulomb force, resulting low probability of interaction with electrons of atomic nuclei. Neutrons interact with both the nucleus and its constituent nucleons. This has several significant effects that may be seen to influence the luminescence phenomenon (Kinchin & Pease, 1955;, 2009). The latter has therefore involve in determining the origin of luminescence and structural defects upon exposure to neutron via FTIR and Raman spectroscopy. Present study could further improve the functionality of borosilicate glass-based radiation dosimeters, especially in thermoluminescence dosimeters.. As a result, a basic knowledge of the radiation's effect may enable borosilicate glass to be used more effectively in a variety of applications, including medical dosimetry in radiotherapy or radiodiagnosis.

1.2   Objectives

The overarching aim of present study is to investigate the borosilicate glass slide as thermoluminescence dosimeter (TLD) for neutron beam applications, detailing further objectives as follow:

1. To characterise the thermoluminescence properties of 1mm thickness of borosilicate glass irradiated by neutron source, including glow curve, dose response, sensitivity and linearity index.

2. To analyse the origin of the luminescence produced by the borosilicate glass slide, use being made of FTIR and Raman spectroscopy when exposed to photon (gamma and X-rays) irradiations.

1.3   Thesis Structure

This thesis is divided into five chapters. Chapter 1 includes the background and objectives of this study. Chapter 2 describes the photon interaction with matter, including photoelectric effect, Compton scattering, and pair production, and neutron interaction with matter. The thermoluminescence dosimetry is discussed too. Chapter 3 explains the methodology involve in conducting the experimental work, such as sample preparation up to sample characterization. Chapter 4 discusses and analyses the results obtained. Finally, chapter 5 concludes the findings from this experiment and suggests several directions for future studies.

CHAPTER 2: LITERATURE REVIEW

2.1 Photon Interaction with Matter

The photons of ionizing radiations, such as gamma and X-rays exhibit narrow wavelength and high frequency. Photons are capable of three fundamental interactions: photoelectric effect, Compton scattering, and pair production.

2.1.1 Photoelectric Effect

The photoelectric effect only occurs with bound electrons and is important with fairly low energy γ or X-rays and heavy atomic number materials. These photoelectric interactions are most probable when the electron binding energy is less than the energy of the incident photon. If the electron binding energy is greater than the photon, the photoelectric interaction cannot occur as the photons need to have sufficient energy to overcome the binding energy in order to remove the electron from the atom. In the photoelectric effect, an incident photon collides with, and transfers all of its energy to an atomic electron. It is considered as an interaction with the atom as a whole, in which the incident photon is absorbed and a planetary electron is emitted with energy equal to the difference between the photon energy and the electron binding energy. These ejected electrons are known as photoelectrons. The photon energy is divided into two parts by the interaction. A portion of the energy is used to overcome the electron binding energy and to remove it from the atom. The rest of the energy is transferred to the electron as kinetic energy (Suliman, 2007) (see equation 2.1).

$$KE = hv - E_b \qquad\qquad (2.1)$$

Photoelectrons tend to be from the most tightly bound shells, producing an inner shell vacancy. Since the interaction creates a vacancy in one of the electron shells, typically the K or L, an electron moves down to fill in. The drop in energy of the filling electron often produces a characteristic X-ray photon. The process is illustrated in Figure 2.1 for photons interacting with inner shell electrons. The mass attenuation coefficient for photoelectric attenuation decreases with increasing photon energy; i.e. as general rule high energy photons

are more penetrating than low energy radiation. For a fixed value of the incident photon energy the attenuation coefficient increases with the atomic number Z of the substance. The probability of photoelectric absorption is determined by a large number of factors, some of which include the kinetic energy of the incoming photon, the electron binding energy, and the atomic number. As a rough estimate of proportionality, the following equation may be used to approximate the likelihood of photoelectric absorption per unit of mass. This equation 2.2 serves as an approximation of proportionality, τ.

$$\tau \propto \frac{Z^4}{E^3} \tag{2.2}$$
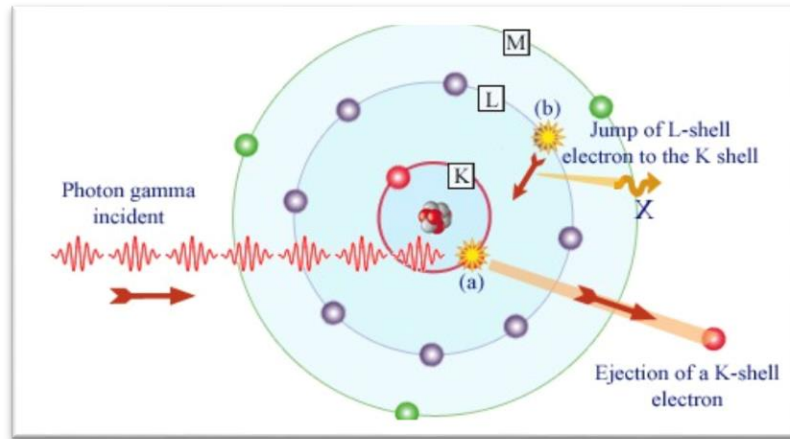
Figure 2.1 Photon absorption by an atom absorption by an atom.

2.1.2 Compton Scattering

This is the process in which γ or X-rays elastically collide with atomic electrons, scattering through an angle θ. In this case, the photon is deflected from its original position, the result of high-energy photon collisions with a target, then releasing loosely bound electrons from the outer shell of the atom. These much greater energies (compared with electron binding energies) make the electrons free and at rest. A portion of energy is absorbed and a photon is produced with reduced energy. The scattered photon has energy less than the incident photon. As the energy is reduced, the frequency will be lower and the wavelength (λ) will be longer, based on Planck relationship.

As seen in Figure 2.2, the incoming gamma-ray photon with energy E is deflected at an angle of with respect to its original path. The electron, which is believed to have began the contact in a state of rest, becomes a recoil electron after acquiring a portion of the energy that the photon had to provide. The interaction between the scattering electron and the target electron causes a portion of the incoming photon's energy and momentum to be dissipated. The remaining energy is absorbed by the dispersed photon. The following equation shows the relationship between the energy of the scattered photon, represented by E', and the scattered angle, indicated by equation 2.3.

$$E\gamma' = \frac{E\gamma}{1 + \frac{E\gamma}{m_o c^2}(1 - \cos\theta)} \tag{2.3}$$

Where Eγ is the energy of the incident photon and $m_o c^2$ is the electron rest mass energy (0.511 MeV)
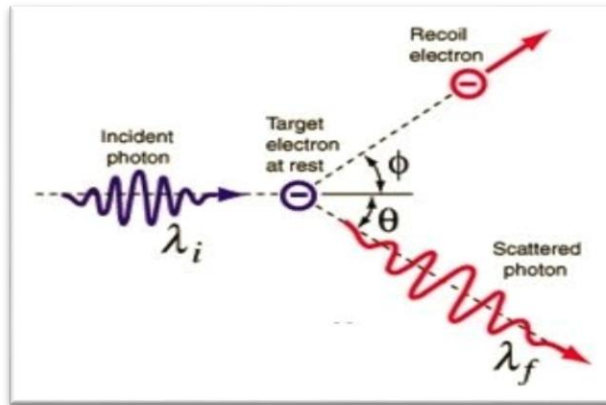
Figure 2.2 Schematic diagram of Compton scattering.

2.1.3 Pair Production

Pair production is the process that results from the transformation of a photon into an electron and positron. This process occurs when a photon interacts with the electric field of a charged particle; however, this interaction is only conceivable if the photon's incident energy is at least 1.022 MeV. This is because the electron and the positron, when stated in terms of energy units (using the E = mc² equation), both have a rest mass of 0.511 MeV. Therefore, the creation of the electron-positron pair is impossible until the requisite

energy threshold of 1.022 MeV is met. If the photon's energy exceeds 1.02 MeV, the electron and the positron will each get a share of the extra energy as kinetic energy.

Once released inside the medium, electrons and positrons are destroyed by their subsequent interactions with other particles. However, the positron's route is not as simple as the electron's, which is rapidly absorbed. As it slows and comes to a halt, it combines with a neighbouring electron, resulting in what is known as annihilation radiation, where the two particles cancel each other out. At this point, the two particles, which are travelling at an angle of 180 degrees to one another and have a combined energy of 0.511 MeV, are transformed back into two photons of electromagnetic radiation, which are either absorbed or dispersed by the medium.

2.2   Neutrons Interaction with Matter

Interactions of neutron with matter, including thermal, epithermal, fast and relativistic neutrons will then be described in this section. Neutrons and protons are the two primary building components of atomic nuclei. Neutrons are electrically neutral, therefore their only contact with nuclei is via nuclear forces. Since it is not a charged particle, it is not necessary to pass through the coulomb barrier while approaching a nucleus. As a direct result of this, neutrons have a greater likelihood of participating in nuclear interactions than charged particles. Neutrons and nuclei are capable of two sorts of interactions: scattering and absorption. The latter is the more prevalent of the two. Neutron and nucleus interact during scattering; nonetheless, both particles are still present after the process. A scattering collision may be represented by a (n, n) reaction or an as reaction as in 2.4.

$$n + {}^{A}_{Z}X \rightarrow {}^{A}_{Z}X + n \qquad (2.4)$$

It is possible for elastic or inelastic scattering to occur. When two particles contact in a manner that results in elastic dispersion, all of their kinetic energy is conserved. In this mechanism, kinetic energy is simply transferred from one particle to another. In the process of inelastic scattering, a part of the kinetic energy is transported to the nucleus, where it is employed as excitation energy. In order to complete the process of returning to its starting condition after the collision, the excited nucleus will emit one or more gamma rays. In the case of absorption, the neutron is destroyed; nevertheless, after the reaction is complete, more particles are created. When a neutron undergoes elastic scattering, it produces a number of distinct types of neutrons, the interactions of which are categorised according to the neutrons' individual energies.

The word "thermal" refers to the state of being in thermal equilibrium and does not imply that anything is necessarily heated. Thermal neutrons are free neutron particles that exist at 300 Kelvin (room temperature) after they have achieved thermal equilibrium with the background atoms. This particle has a very low energy level (approximately 0.025 eV), yet it is essential to the functioning of a thermal nuclear reactor because it enables more effective neutron absorption throughout the chain reaction (fission or radiative capture) (Kozima, 2006).

A neutron with fission energy that has had part of its velocity retarded by the moderating process but has not yet attained thermal energy is an epithermal neutron. Multiple resonance peaks are often seen in the epithermal energy spectrum, which may vary from a few eV to 100 eV for neutron capture and the induced neutron fission process, especially with U-235. This is less significant in quick neutron processes because neutrons are more likely to be absorbed before entering the slowing phase (moderation).

As for the fast neutron, during nuclear fission, a thermal neutron combines with the atomic nuclei of an atom, such as U-235, producing a radioactive atom with unstable nuclei, such as U-236. When an unstable neutron nuclide decays and turns into a stable

nucleus, accompanied with the release of energy and neutrons, fission begins. This is the first stage in the chain reaction of fission. These neutrons are considered fast neutrons due to their energy range of 0.1 MeV to 20 MeV and their speed of 14,000 km/s, which is about 5% of the speed of light.

As per neutron that exhibits relativistic effects, as secondary particles, high-energy neutrons with a lower energy than fission-produced neutrons may be generated in a particle accelerator. In contrast, the particle energy of protons and deuterons that originate from alpha and heavy ions may be up to 20 MeV higher. Due to the cosmic radiations prevalent in the universe, the relativistic neutron may be contained in the atmosphere.

2.3   Thermoluminescence dosimetry

2.3.1   Luminescence

Luminescent phenomena have held the attention of humans ever since the beginning of time. There are several examples of naturally occurring luminescence, such as the light emitted by glow worms and fireflies, and the luminescence produced by a variety of marine microbes and deep-sea animals. Because of this, this phenomenon has, from the very beginning, piqued the interest of scientists from all over the world who work in various fields such as geology, chemistry, physics, and the biomedical sciences, as well as those involved in various industrial applications for quality control and research and development. The reason luminescence is of such importance in the modern world is that it is fast replacing conventional lighting in business settings and also serving as a medium for human communication via the use of television screens. In addition to this, it played an essential role in the discovery of radioactivity, electrons, and x-rays (Harvey, 2011).

The distinguished German scientist Eilhard Wiedemann first introduced the term "luminescence" in 1888 to designate a luminous emission that is not simply thermal in origin, i.e. Luminescence as "cold light," or light from other sources of energy, occuring

at normal and lower temperatures. Some energy sources, when given additional energy, enable the ejection of electrons from atoms from their ground state (state of lowest energy) into excited states. These excited states have a higher energy than the ground state (states of greater energy). Because these excited states are unstable, electrons may return to the ground state by releasing this boosted energy in the form of light as they return to the ground state. This occurs because these excited states are not stable (Harvey, 2011).

Luminescence is another term for the emission of light from a solid, which occurs as a result of the release of energy that has been stored as a result of certain types of previous incident radiation (DeWerd & Stoebe, 1972). There are three unique forms of luminescence, and they are called fluorescence, thermoluminescence, and phosphorescence. Despite the fact that they share many traits, they are brought on by entirely different mechanisms . Both fluorescence and phosphorescence are dependent on the time delay between light absorption and emission; the process is referred to as fluorescence if the luminescence occurs during the time that the excitation irradiation is active, and it is referred to as phosphorescence if the luminescence occurs after the excitation irradiation has ceased. Fluorescence and phosphorescence are both dependent on the time delay between light absorption and emission (DeWerd & Stoebe, 1972). For fluorescence, which happens when light is absorbed and re-emitted at different wavelengths, this period is less than 10^{-8} seconds. Fluorescence occurs when light is absorbed and re-emitted. Because of the molecule's ability to disperse energy in many different directions, the light that is emitted has a longer wavelength than the light that is absorbed (Furetta, 2003). In the case of phosphorescence, this phenomenon takes place when energy is absorbed and then re-emitted after a length of time that is more than 10^{-4} seconds after the absorption process has come to an end. The phosphorescence process may be described as being characterised by the presence of a metastable level that acts as

an electron trap between the basic level and the excited level (Furetta, 2003). In addition to the factors described above, the process may also be the result of an adequate source of stimulation, which is typically either light or heat. The phenomenon is referred to as optically stimulated luminescence (OSL) when the exciting agent is light; however, when the exciting agent is heat, it is referred to as thermoluminescence; in the latter case, the material could form the basis of a thermoluminescence dosimeter (TLD) if it was used for radiation dosimetry purposes (Izewska & Andreo, 2000)

2.3.2   Thermoluminescence

Sir Robert Boyle empirically defined thermoluminescence (TL) in a 1663 report to the Royal Society, describing how, upon warming a diamond in contact with his body, he saw luminescence in the dark (Rivera, 2012).

Thermoluminescence (TL) is the phenomena in which a TL material previously subjected to penetrating radiation generates light under heat. The method has been used for decades to measure the energy deposited in a material after irradiation. The approach is flexible, responding to, proton, and -particles as well as UV, x-, and -rays and neutrons. TSL is the cornerstone of thermoluminescence dosimetry (TLD) (Furetta, 2003),a passive kind of detection used to date archaeological material, analyse environmental exposure, and evaluate medical irradiation and radiation processing doses.

TLD began in 1895, when W. C. Roentgen discovered X-rays. These radiations may create luminescence in some materials, especially those containing manganese as an impurity. Calcium fluorite and calcium sulphate are employed to detect ionising radiations. E. Wiedemann and G. Schmidt employed thermoluminescence (TL) to detect 'cathode rays,' the name for electron beams before the electron was visible (Kron et al., 1999). F. B. Daniels (Daniels et al., 1953) from University of Wisconsin describes the evolution of TLD in medicine. He mentioned geological dating and described what

appears to be the first clinical application of LiF: "The crystals were swallowed by the patient (who had received a radioactive isotope injection), recovered one or two days later, and the accumulated dosage in roentgens was measured by matching thermoluminescence intensity with a known roentgen dosage" (Daniels et al., 1953)

2.3.3 TL Mechanism

After discussing the background and history of thermoluminescence, the mechanism of thermoluminescence will be discussed. The most prevalent explanation for the TL phenomena is the band model, which is based on the energy band theory in insulators (McKeever et al., 1995). The band model illustrates a valence band in which electrons may easily flow, a conduction band in which electrons are linked least firmly, and a band gap for a crystal devoid of lattice imperfections. There are no possible energy levels for electrons to occupy between these bands. A band gap, also known as a forbidden gap or a mid gap, is the space between the valence and conduction energy bands. This gap is also referred to as a banned gap and a mid gap. This area has the potential to develop defects, which may have been caused by radiation or existing contaminants. Radiation-induced defects are non-equilibrium concentrations of electrons occupying localised electronic states (Furetta, 2003). It is commonly believed that the TL medium has two kinds of impurities, electron traps and hole traps, which are localised at mid-gap states. This is indicated in the description of the TL event (McKeever et al., 1995). In the mid-gap, it is assumed that the electron trap is close to the valence band, but the hole trap is located far from the valence band.

When thermoluminescent materials are subjected to ionising radiation, free electrons and holes are produced. Electrons may travel from the valence band to the conduction band when thermoluminescence materials are triggered by ionising radiation. Positive hole describes the void generated in the valence band. Electrons and holes may move freely

along their respective bands until encountering the electron and hole traps (E and H, respectively) (H). The luminescence centres (L) in this process are referred to as the hole traps (McKeever et al., 1995).

The amount of energy needed for electrons to escape is influenced by a number of variables, including the traps' depth and the material's temperature. Before the trapped electrons may recombine with the holes in the luminescence centre, they must be stimulated into the conduction band. This requires a suitable temperature (L). Photons are released into the environment as a result of the recombination of electrons and holes. This particular hole trap is referred to as a recombination centre (R. Chen & McKeever, 1997). As the temperature increases, there is a corresponding increase in the amount of excitation, resulting in a further release of the stored energy and a transition from the metastable to the ground state. During this process, any excess energy will be emitted as either visible or ultraviolet photons, which may be measured by photomultiplier tubes.

The temperature necessary to release a trapped electron and create thermoluminescence is determined by the energy gap between the conduction band and the trap (Townsend, 1990). By measuring the intensity of the emitted light, the quantity of charge that has been discharged may be determined. This intensity is proportional to the dosage received, and one would generally anticipate that the quantity of radiation exposure would influence the amount of light emitted. The term "thermoluminescence glow curve" refers to the connection between temperature and light emission (R. Chen & McKeever, 1997). When assessing dosage, the region below the major glow curve is evaluated. In the majority of cases, the layout of the glow curve will look as one or more overlapping peaks of emitted light. Several factors, such as the spectrum sensitivity of the light-sensitive device, the heating rate, and the use of various filters between the sample and the detector, influence the magnitude of this overlap (Hanna, 1978). The basic one-trap one-

recombination centre (OTOR) shown in Figure 2.3 is the core model used to describe the

behaviour of TL. This structure is referred to as the one-trap one-recombination centre

(OTOR) (Ying et al., 2012).
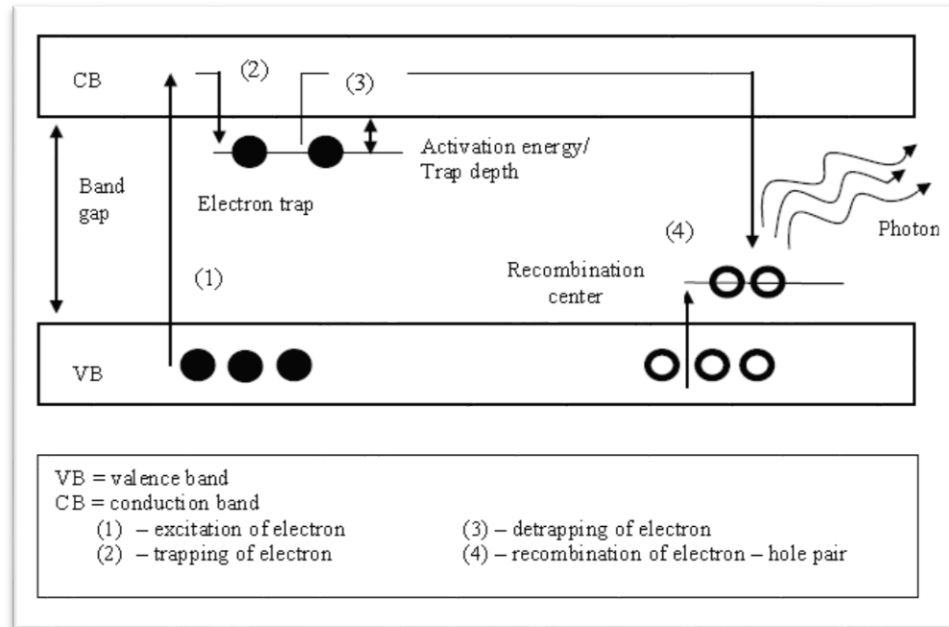
Figure 2.3 Diagram showing a simplified model of one trap and one recombination centre (OTOR).

CHAPTER 3: METHODOLOGY

3.1   Thermoluminescence

3.1.1   Sample Preparation Process

The samples used in this project is borosilicate glass slide with 1.0 ± 0.01mm thickness of two different brands; Silane and HmBg (see Figure 3.1). The sample was cut into dimension of $(0.5 \times 0.5) \pm 0.1$ cm^2 by using glass diamond cutter (see Figure 3.2). The cut glass was examined to make sure that there is no unmatched crack at the edge of the glass square so that it will not disturb the result when reading was taken using TLD machine.

Figure 3.1 Diagram showing borosilicate glass slide of 1mm thickness with the brand of silane [on the right] and with the brand of Hmbg [on the left].

Figure 3.2 Diagram showing a piece of cutted borosilicate glass slide with the dimension; $(0.5 \times 0.5) \pm 0.1$cm^2.

3.1.2 Annealing Process

The TL dosimeter glass slides were annealed in order to remove any filled flaws, including those caused by irradiation, tribo- and chemo-luminescence, standardize the temperature history and sensitivity, stabilize the trap structure, and return them to the circumstances that existed prior to their initial use. To accomplish these objectives, annealing was conducted. The samples were confined inside a ceramic plate and wrapped in aluminium foil (C. Chen et al., 2015). This was done to avoid contamination from the multi-user furnace and to decrease the possibility that samples would be lost. In a furnace as seen in Figure 3.3 (Micro-controller X; model PXR4/5/7/9) maintained at 400 °C, the borosilicate glass was annealed for one hour. The samples were then kept in the furnace for 18 hours, after which they were progressively cooled to room temperature to minimise the effects of thermal stress unrelated to irradiation. In this regard, rapid cooling may lock in the high-temperature equilibrium of isolated defects, while gradual cooling can lead to a variable but lower degree of defect aggregation. This is possible due to the fact that fast cooling may freeze the high temperature equilibrium of isolated faults. It has been shown that variations in the rate of cooling may influence the reported trapping parameters and TL sensitivity in certain TL materials (McKeever et al., 1995). The samples were then placed in an opaque, light-resistant plastic container so that they could be handled according to protocol.

Figure 3.3 Furnace (Micro-controller X; model PXR4/5/7/9)

3.1.3 Irradiation Process

In this particular irradiation method, the samples are subjected to three different types of irradiations, including neutron, gamma-ray and X-ray. Neutron irradiation was performed at the Nuclear Malaysia Agency in Bangi, Selangor, while gamma and X-ray irradiation were carried out at the Department of Physics at the University of Malaya.

Figure 3.4 shows the gamma irradiator cell which comprises annular source that is permanently contained inside a lead shield, a cylindrical drawer, and a drive mechanism that can move the drawer up or down along the source center-line. The Gamma cell has a radionuclide called ^{60}Co, which emits two different photon intensities (1.1732 MeV and 1.3325 MeV). The predetermined dosage can be calculated by using the dose rate as in equation 3.1 below.

$$D_t = D_0\, e^{-\lambda t} \tag{3.1}$$

where D_t is the dosage rate in Gy/s, D_o is the starting dose rate ($D_o = 0.525$ Gy/s) in November 1995, λ is the decay constant with a value of $4.1681 \times 10\text{-}9$ s^{-1}, and t is the time difference between November 1995 and the current day in seconds. The initial radiation rate is found to be 0.525 Gy/s. The length of time that has passed since November 1995 and compare it to the current moment, the D_t value for a needed dosage is found to be 1.5 Gy/min. Calculated as follows by applying equation in 3.2 and 3.3 to the given data.

$$D_t = \frac{D}{t} \tag{3.2}$$

$$t = \frac{D}{D_t} \tag{3.3}$$

Where t is the time control expressed in seconds and D is the needed dosage expressed in Gy, respectively.

Table 3.1 Time exposure to required dosage

Dose (Gy)	Time exposure (minutes)
2 Gy	1.2 minutes

Figure 3.4 ^{60}Co Gammacell at the radiation laboratory of Physics department.

In addition to the processes outlined above, borosilicate glass was exposed to X-ray beams from an ERESCO 200 MF4-RW (see Figure 3.5) at a dosage of 2 Gy located at the Department of Physics, University of Malaya. Inside the X-ray machine, one may find an X-ray tube. An X-ray tube is a fairly simple electrical component consisting of an anode, a cathode, and a vacuum-sealed container for the two. Tungsten, which has an atomic number of 74, is utilized in the target of an X-ray generator, and the component that produces the X-rays is known as the anode. Due to its high melting point and relatively slow evaporation rate, tungsten has a variety of remarkable properties, the most prominent of which is its ability to be kept at high temperatures.

Figure 3.5 ERESCO 200 MF4- RW X-ray source

The cathode, which is a filament that is heated, creates a flow of electrons as a result of a current that is supplied through the cathode filament, causing it to become heated. From the cathode to the target, also known as the anode, electrons travel via the tube. Due to the large voltage difference between the cathode and anode, these electrons have a substantial amount of energy as they move down the tube. When electrons travelling at high speeds collide with tungsten atoms, they may eject electrons from orbitals of lower energy. Higher orbital electrons fill previously free locations, so releasing extra energy

as X-ray photons. Electrons also lose momentum due to Coulombic interactions, leading to the emission of bremsstrahlung or X-ray radiation.

In addition, the samples were also subjected to neutron radiation at the TRIGA PUSPATI Reactor administered by the Malaysian Nuclear Agency (see Figure 3.6). The small core of the reactor makes it possible to attain a critical mass and larger neutron fluxes while maintaining an extraordinarily high level of safety. Neutrons were exposed to the samples at doses of 2, 4, 6, 8, and 10 Gy throughout the treatment period. Pneumatic Transfer System (PTS) (see Figure 3.6 (a)) is a pneumatically controlled "rabbit" transfer system that enables the production of very short-lived radioisotopes for neutron activation research. It enters the core lattice of the reactor at point G-20. The pressure difference created by air suction acts as its major control mechanism. The pressure within the system is never equal to the air pressure outside the system; rather, it is always lower. Even if there is a leak, radioactive materials will not be released into the surrounding environment.
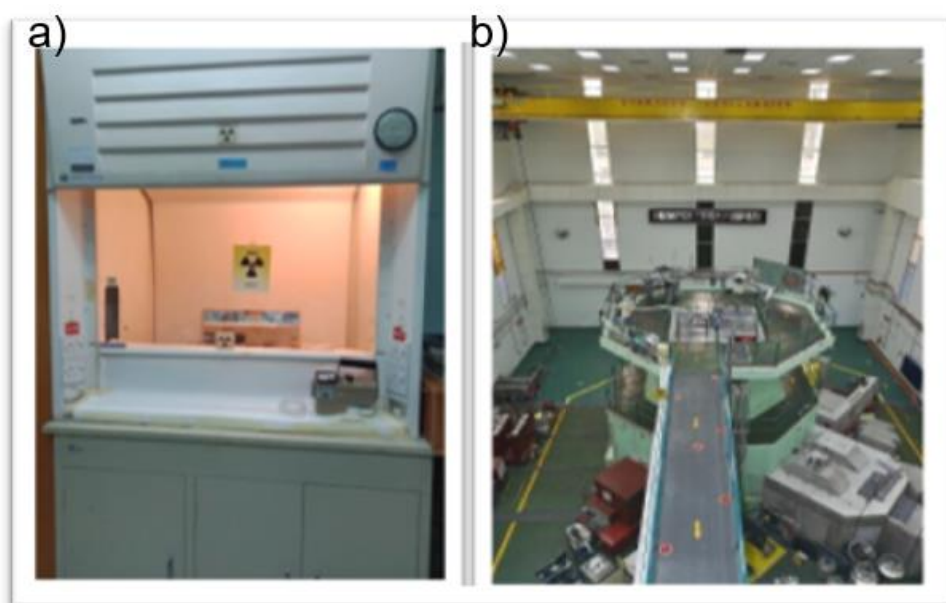
Figure 3.6 Pts control station positioned adjacent to the fume cupboard and the TRIGA PUSPATI Reactor

3.1.4 Sample Readout

Using a Harshaw 3500 TLD reader available in the Physics Department of the University of Malaya (refer Figure 3.7), readings on borosilicate glass were obtained. The employed TLD reader is supported by WinREM's software, and the whole setup comprises of a photomultiplier tube (PMT) in a light-tight chamber, as well as supporting facilities, such as an electrometer for recording the PMT signal as a charge or current. The PMT in the TLD reader plays a crucial role in detecting the TL light emission and turning it into an electrical signal that is proportionate to the observed photon fluence. In addition, a TLD reader photomultiplier tube with a fixed location in the centre is so that the arrangement may be seen using it. During the process of data reading, a slow flow of nitrogen gas is fed to the equipment. This is done in part to minimize oxidation of the material and also to eliminate the impact of chemiluminescence and triboluminescence. According to (McKinley, 1981) the mechanical disturbance of the surface produces triboluminescence. Under the present circumstances, this raises problems with the process of cutting glass into minute square bits (Bull, 1986).

For this work, the TLD reader's readout system was set with the following parameters: A preheat temperature of 50 ºC for 40s, followed by a ramping to a maximum temperature of 350 ºC during data gathering due to a heating rate cycle of 10 ºCs^{-1}. The optimal TLD reader settings for obtaining a light curve devoid of the effects of superficial traps have been determined (flushed out by the pre-heat cycle). In order to determine the time–temperature profile (TTP) that permits complete capture of the TL glow curve under optimal conditions, the heating rate cycles, also known as the ramp rate, have been altered in a variety of ways. After the reading method was completed, the TL values for each dosimeter were normalised to the dosimeter mass, and the results were produced in nC/mg.

Figure 3.7 Harshaw 3500 TLD Reader located at the Radiation Laboratory of Physics Department.

3.2 Optical Characterisation

3.2.1 Fourier transform infrared (FTIR) Spectroscopy

In the Department of Chemistry at the University of Malaya, Fourier-transform infrared spectroscopy (FTIR) measurements were carried out using a Perkin Elmer (FTIR-Spectrum 400) in the range between 400 and 4000 cm^{-1} to identify the functionalization of silica structures that present in borosilicate glass slides. The interaction of matter and electromagnetic fields in the infrared radiation (IR) area is the focus of infrared spectroscopy, which is conducted as a function of photon frequency. The fourier transfer infrared spectroscopy (FTIR) diagram for the comprehensive analysis procedure of the sample that has been subjected to infrared radiation can be seen in Figure 3.8. In the first place, an infrared energy beam may be produced by a luminous black-body light source. The infrared beam is then directed into the interferometer, which is responsible for the generation of the interferogram signal. Following that, the beam travels through the sample and into the sample compartment, where it is either absorbed by the sample or reflected by the surface of the sample. Molecules of the sample absorb infrared radiation at certain wavelengths when the sample is subjected to infrared light, which causes a change in the dipole moment of the molecules. When materials are subjected to infrared

radiation, molecules of the sample absorb in the sample allows part of the infrared light to pass through it, while at the same time absorbing some of it. Because of this, the vibrational energy levels of the molecules in the sample go from their ground state configuration to their excited state configuration. The resultant spectrum reveals the amount of light that is transmitted through and absorbed by the molecules of the sample, so producing a molecular fingerprint for the sample. The vibrational energy gap of sample molecules may be calculated based on the frequency of the absorption peak, and the number of the absorption peak corresponds to the number of vibrational freedoms possessed by the molecule. The potential of a transition between energy levels and the change in dipole moment both have a role in determining the amplitude of the peak of absorption. Finally, the infrared beam makes its way into the detector for one more set of measurements. The signal that was measured is digitized and then delivered to the computer so that it may be transformed using the Fourier method. The user is then given with the finished infrared spectrum for interpretation and any further processing that may be necessary.

The Fourier transform infrared spectroscopy (FTIR) provides useful information on the rotation and vibration of molecular structures as well as the state of chemical bonding in the materials, which facilitates the investigation of inorganic as well as organic substances. In addition to this, an infrared spectrum gives information about a sample's fingerprint by revealing absorption peaks that are related with the frequency of vibrations between the bonds of the atoms in the sample. There is no pair of materials that may produce an infrared spectrum that is identical to one another since each substance is made up of a distinct atomic makeup. Therefore, it is possible for infrared spectroscopy to result in the identification of materials. In addition, the FTIR allows us to determine the composition of a material, identify previously unknown elements, and quantify the

amounts of individual components in a combination. The absorption of a single chemical is expressed as a function of the frequency for any medium that is homogenous as follows:

$$A = a \times b \times c \qquad (3.4)$$

Where A refers to the measured sample absorbance at the given frequency, a represents for the molecular absorptivity at the given frequency, b means the path length of source beam in the sample, and the concentration of the sample is denoted as c (Griffiths & De Haseth, 2006) . It is indicated that there is a linear proportional between the concentration of every component in a solution or homogeneous mixture and the intensities of absorption bands by this law (Mayerhöfer et al., 2020).

Figure 3.8 FTIR spectroscopy located at the department of chemistry

3.2.2   Raman Spectroscopy

The method of Raman spectroscopy is helpful for identifying a variety of substances, including solids, liquids, and gases. It is an easy-to-use, non-destructive method that requires no sample preparation. An optical method called Raman spectroscopy relies on the inelastic scattering of monochromatic light, often from a laser source. When interacting with a sample, photons in monochromatic light experience inelastic scattering, which modifies their frequency. The sample absorbs photons from the laser light, which are subsequently reemitted. The Raman Effect refers to the frequency shift of the

reemitted photons relative to their initial monochromatic frequency. This shift reveals details on the vibrational, rotational, and other low frequency transitions that take place in molecules. This phenomenon is based on molecular deformations in an electric field, E, which is controlled by the polarizability of the molecules, (α). The Stokes and anti-Stokes lines are similarly spaced from the Rayleigh line (see figure 3.9). This happens because one vibrational quantum of energy is either acquired or lost in both scenarios. Additionally, observe that the anti-Stokes line is substantially weaker than the Stokes line. Because only molecules that are vibrationally stimulated prior to irradiation may produce the anti-Stokes line, this happens. The stronger Stokes line is hence the sole one often examined in Raman spectroscopy. Raman spectroscopy examines molecular transitions in a different way than infrared absorption spectroscopy, which is another vibrational method used to study molecular structure. Raman spectroscopy is very flexible and may be used to analyse a variety of materials in liquids, solids, and gases. Raman spectroscopy may be used to identify unknown substances' chemical composition because of the distinctive spectra that certain types of materials emit as a result of their structural arrangement. Raman spectroscopy is therefore perfect for analysing the quality of materials.

Raman Spectroscopy is a crucial method for characterising the microstructure of glass materials, particularly the investigation of structural defect and in-plane crystallite size, La. In this work, the Raman spectra of borosilicate glass slide material was evaluated using a confocal microscope and a LABRAM-HR Evolution Raman Spectrometer (see Figure 3.10) at room temperature. In a Raman instrument, a laser beam is used to light a sample (argon laser with wavelength 514 nm and power 2.14 eV). A lens collects light from the lighted spot and transmits it via an interference filter or spectrometer to produce the Raman spectrum.
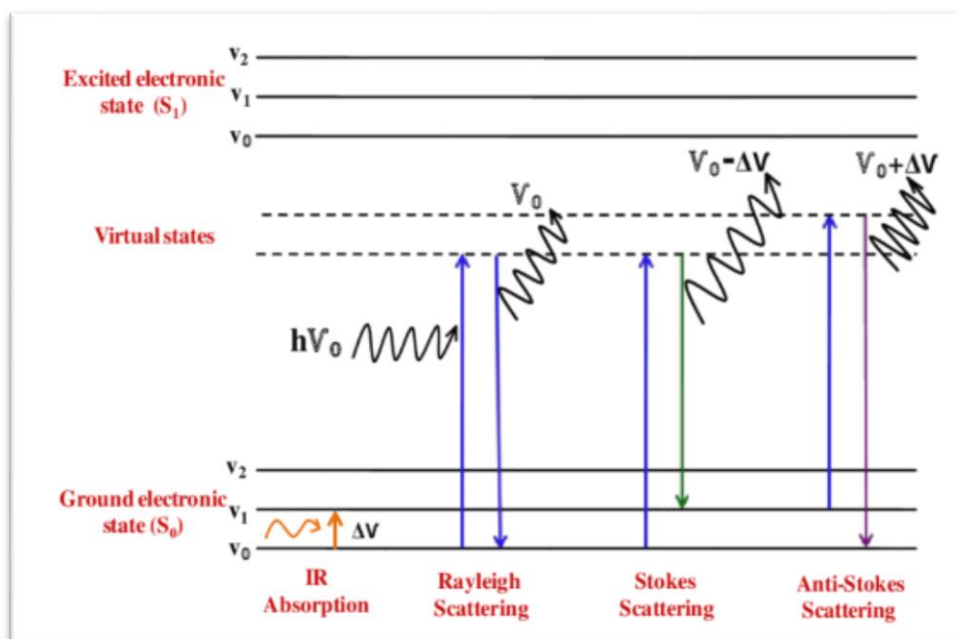
Figure 3.9 Vibrational level of the material

Figure 3.10 A LABRAM-HR Evolution Raman Spectrometer (RENISHAW Model)

CHAPTER 4: RESULT AND ANALYSIS

4.1   Thermoluminescence

4.1.1 Glow Curve

The glow curve is a plot of the intensity against the temperature (see Figure 4.1), that is created during the readout (McKeever et al., 1995).The kind and quantity of the lattice flaws and impurities that are present in the material will affect the form of the glow curve that is produced by the material. In addition, the curvature of the glow curve may be affected by high-dose pre-irradiation, the annealing process, and Linear Energy Transfer (LET). In addition, it is vital to be aware of and educate oneself about the fact that the glow curve will alter based on the heating rate and temperature (Yaakob et al., 2011).In the event that the rate of heating is increased, the maximum glow peak temperature, denoted by Tm, will be elevated to a higher temperature (McKeever et al., 1995).The quantity of deposited radiation energy is equivalent to the number of electrons that were liberated from electron traps, which is represented by the region under the glow curve. Maximum of the light peak shows the greatest amount of electrons liberated from traps. Both the area and the maximum glow peak temperature, T_m, are controlled by a mix of intrinsic and external characteristics, such as the heating rate and the quantity of absorbed energy. By analysing the light curve, the previously indicated trapping charge may be determined.

The glow curve will illuminate the properties of the TL material and provide valuable information. In light to this, the high-temperature TL peaks correspond to deep trapping levels, requiring high temperatures to liberate trapped electrons and are consequently stable at ambient temperature. Low-temperature TL peaks, for instance, correspond to traps in the conduction band, which tend to lose signal with time even when kept at ambient temperature.

It has been observed that the stable peak temperature is obtained in 1 mm (silane) for all dose range, except at 2 Gy, covering the temperature region between 180 to 250 ℃ as shown in Figure 4.1 (a). In contrast to 1 mm (HmBg), the stable peak temperature is appeared for 4 and 6 Gy doses of neutron irradiation (refer Figure 4.1 (b)).

Glow curve studies TL emission is related to the presence of luminescence centres occupied by charge carrier produced during radiation exposure. The area under graph represents the number of electron trap while the glow peak maxima represent the maximum number of electron trap. The maximum intensity peak of glow curve is directly proportional to dosage supplied (Alawiah & Hairul, 2015).

With increasing dosage, more electrons are stimulated to the conduction band and trapped at electron trap sites. Nevertheless,as seen from Figure 4.1(a) ,for 1mm (Silane),the glow curve at dose 6, 8 and 10 Gy is not increasing with the dose ,due to inhomogeneity of defect present in the borosilicate glass slide (Nazeri et al., 2021; Sani, Othman, et al., 2020a; Zubair et al., 2021). The wide and broader glow curve is due to the incorporated and imbalance ions inside the borosilicate glass (Kumar et al., 2020). As seen from Figure 4.1(b),for 1mm (Hmbg), the general glow peak maxima is lower than that of 1mm (silane)(compare with Figure 4.1(a)), thus can be concluded that it is easier (lower energy required) for the electron inside the electron trap of the 1mm (Hmbg) to jump out of the electron trap when heat energy being supplied in comparison to 1mm (silane) (Kumar et al., 2020; Sani, Othman, et al., 2020).
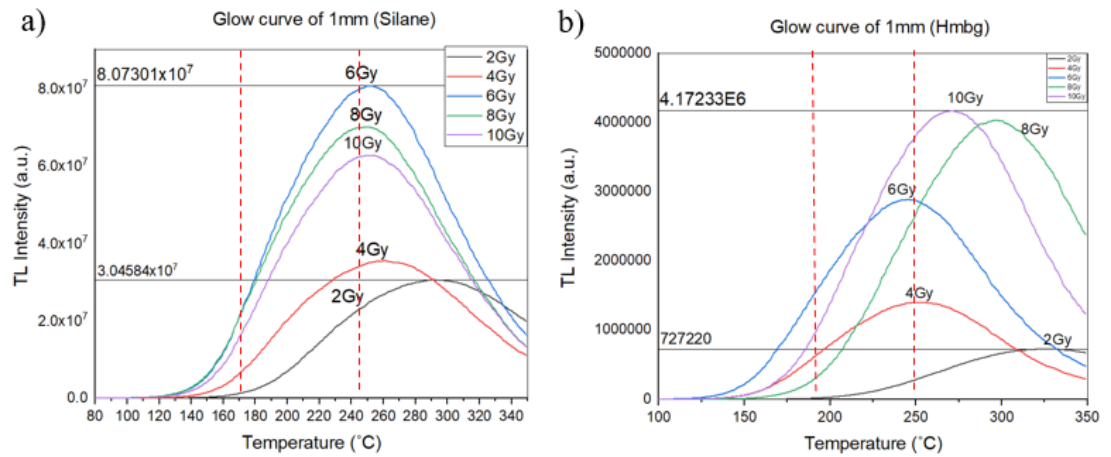
Figure 4.1: Glow curve graph of 1mm (Silane) and glow curve of 1mm (Hmbg).

4.1.2 Dose Response

According to the Figure 4.2, the dose response of 1mm (silane) spans from 1.5×10^{-6} to 7.5×10^{-6} nC which is higher than 1mm (Hmbg) that ranges from 25×10^{-3} to 290×10^{-3} nC. Both graph shows linearity trend over the increase in dose and the TL response is tabulated in Table 4.1. This may be shown by the linear TL response, which supports the results from the earlier research (Alawiah et al., 2015; Bradley et al., 2020; Fadzil et al., 2017; Hashim et al., 2010, 2015; Nazeri et al., 2021; Saeed et al., 2018; Sani et al., 2021; Sani, Othman, et al., 2020). For medical dosimetry, it is required to have the linearity that varies not more than 3% (1SD) (Rivera, 2012). The dose response of 1mm (Hmbg) have the dose response linearity of less than 3% (less than 1 standard deviation) with linear regression close to 0.97 which validate the statement above thus it is suitable as medical dosimeter (see Figure 4.2). It can be shown that the sample dosage response to the TL that is created on glass is proportional to the sample exposure dose (Hashim et al., 2010). When the TL is normalised, a dosimeter of any merit has to have a response that is linear. When attempting to determine the sensitivity of the dosimeter, the dose rate is the single most essential aspect that should be taken into consideration. When working within their range, dosimeters must avoid reaching saturation levels at any time (Hashim et al., 2015).
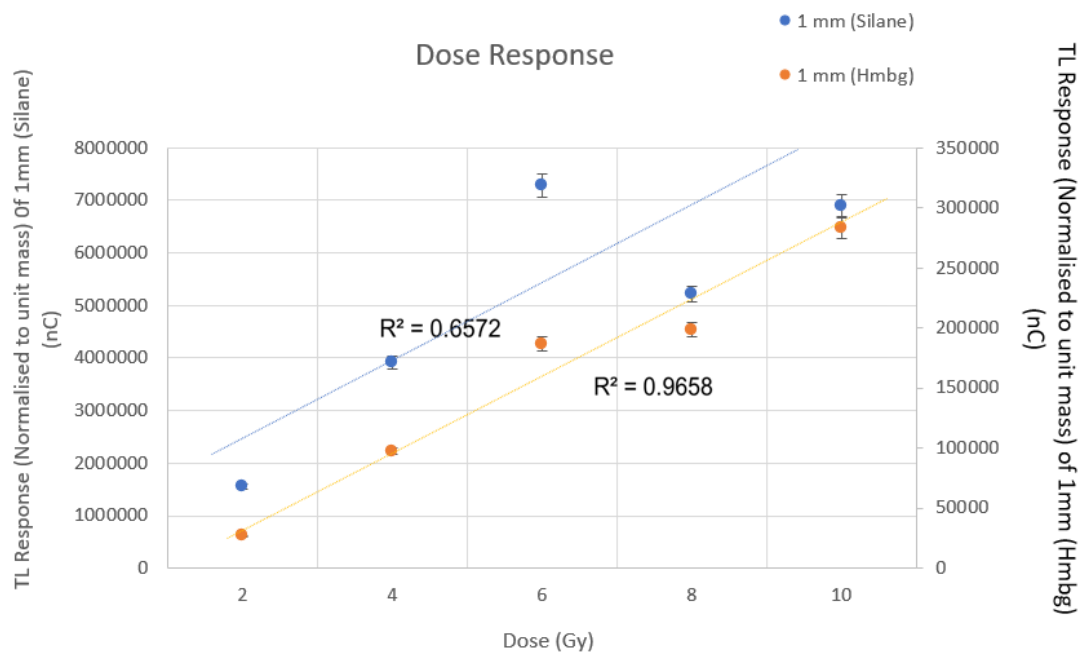
Figure 4.2 Dose response graph 1mm (Silane) and 1mm (Hmbg)

Table 4.1 Table shows the data needed for dose response graph 1mm (Silane) and 1mm (Hmbg)

| Sample (Brand)	Neutron dose (Gy)	TL Response of (nC)
1mm (Silane)	2	1552574.775
	4	3915262.042
	6	7280393.649
	8	5220386.819
	10	6901173.532
1mm (Hmbg)	2	26735.48792
	4	97570.98431
	6	186703.3068
	8	198547.0588
	10	283338.5116

4.1.3   Sensitivity

The amount of light that is designed to respond to a certain dosage of incoming radiation is what establishes the level of sensitivity. The dosimeter's light output per dosage unit measurement is used in the process of quantifying the TLD radiation sensitivity. The sensitivity of the TLD components and the translucence of their Teflon® coating both have a role in determining the amount of light that is emitted by the TLD. The sensitivity of the TL may be expressed as the TL intensity per unit dose per unit mass of sample. This value is affected not only by the activator concentrations but also by the defects in the sample.. It is reasonable to assume that the borosilicate glass will have a high level of energy exchange efficiency if it contains a substantial number of hole and electron traps(Kraevskii, 2001; Vance, 2003). Even if they come from the same batch, individual dosimeters may have varying degrees of sensitivity due to variables such as variances in detector mass and surface impurities (Furetta, 2003). This sensitivity can be calculated by the equation 4.1 below.

$$Sensitivity = \frac{TL}{D.m} \qquad (4.1)$$

From the Figure 4.3, it can be observed that the sensitivity of 1mm (silane) is highly sensitive compared to 1mm (Hmbg). The details is tabulated in Table 4.2. From the graph of 1mm (silane) from (2 to 6Gy) is from 700×10^{-3} to 1.20×10^{-6} nC.Gy^{-1}.g^{-1} and goes down to 650×10^{-3} nC.Gy^{-1}.g^{-1} (8Gy) and goes up to 700×10^{-3} nC.Gy^{-1}.g^{-1} (10Gy). For 1mm (Hmbg) , from (2 to 6Gy) is from 14×10^{-3} to 31×10^{-3} nC.Gy^{-1}.g^{-1}, then goes down to 25×10^{-3} nC.Gy^{-1}.g^{-1} (at 8Gy) and rises to 28×10^{-3} nC.Gy^{-1}.g^{-1}. Basically the graph fluctuate from 2 Gy to 6 Gy and goes down to 8 Gy and rise up to 10 Gy with uncertainty below than 1 standard deviation. The low optical signal that occurs at these dosages, which results in a high signal-to-noise ratio, is the cause of the difference in sensitivity

that occurs at the higher dose (Ibrahim et al., 2016; Kraevskii, 2001; Patra et al., 2016; Xu et al., 2014).
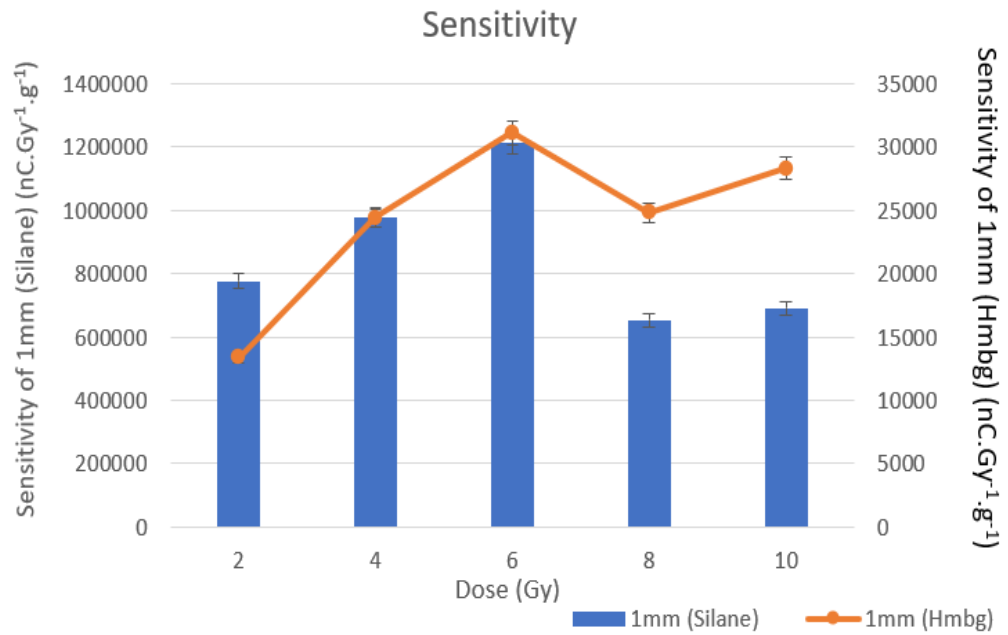
Figure 4.3 Sensitivity graph of 1mm (Silane) and 1mm (Hmbg).

Table 4.2 Table shows the data needed for Sensitivity graph of 1mm (Silane) and 1mm (Hmbg)

Thickness,mm (Brand)	Dose (Gy)				
	2	4	6	8	10
Sensitivity of 1mm (Silane) $(nC.Gy^{-1}.g^{-1})$	776287.3875	978815.5104	1213398.9420	652548.3524	690117.3532
Sensitivity of 1mm (Hmbg) $(nC.Gy^{-1}.g^{-1})$	13367.7440	24392.7461	31117.2178	24818.3824	28333.8512

4.1.4 Linearity Index

The normalised thermoluminescence (TL) dose response may be easily determined using the linearity index (D). The relevance of the index stems from the fact that an ideal dosimetric material should have a dose response that is linear throughout a large dosage range (Abdul Sani, et al., 2020). This is where the index gets its meaning. On the other

hand, not all of the dosimetric materials that are utilised in practical dosimetry display this trait; rather, they exhibit a wide range of non-linear effects. When the dose of a TLD material is increased, for example, the response is usually linear, then supralinear, and finally sublinear (McKeever et al., 1995). This is due to the fact that the supralinear response is often associated with high radiation doses that induce damage to the medium and generate more traps, while the sublinear response is expected to take place when the TL material approaches saturation in the electron-hole traps (Böhnke et al., 2015; Gouget-Laemmel et al., 2013; Sani et al., 2021; Sani, Othman, et al., 2020) .In addition to that, it's possible that the non-uniform spatial ionisation density that occurs after electron irradiation is the root of this problem. The Unified Interaction Model (UNM) has been developed to adequately represent this phenomenon (Hashim et al., 2015) Using the formula below , linear behaviour is achieved when f (D) equals 1, whereas the response is deemed to be superlinear when f (D) is more than 1, and it is regarded as sublinear when f (D) is lower than 1 (Rivera, 2012).

$$f(D) = \frac{\frac{M(D)}{D}}{\frac{M(D_1)}{D_1}} \qquad (4.2)$$

where :

M (D) = The intensity of TL signal at dose, M (D_1) = The intensity of TL signal at low dose , D = Dose , D_1 = Low dose

It is apparent that 1mm (silane) shows linearity which is f(D) = 1 at (2Gy), at (4,6Gy); supralinearity, at (8,10 Gy); sublinearity (see Figure 4.4). The details is tabulated in Table 4.3. while 1mm (Hmbg) shows supralinearity at (4,6,8,10Gy).The linearity index value as shown in the Figure 4.4 varies respectively at certain doses with the error bar of not more than 1 standard deviation. The least detectable dosage is represented by the point

at which the linear section begins, and the maximum detectable dose is represented by the point at which it ends. The lowest detectable dosage is mostly dependent on the grain size of the sample; specifically, the minimum detectable dose rises as the grain size of the sample becomes smaller. However, the low detectable dose is primarily dependent on the heat treatments and evaluation procedures in order to eliminate the residual dose (also known as zero dose or unirradiated readout) and reduce the standard deviation of this value in order to minimise the low detectable dose (Alqahtani et al., 2020; Boffy et al., 2016; Zubair et al., 2021). This is done in order to minimise the amount of radiation that is absorbed by the patient (Nabil El Faramawy et al., 2013).
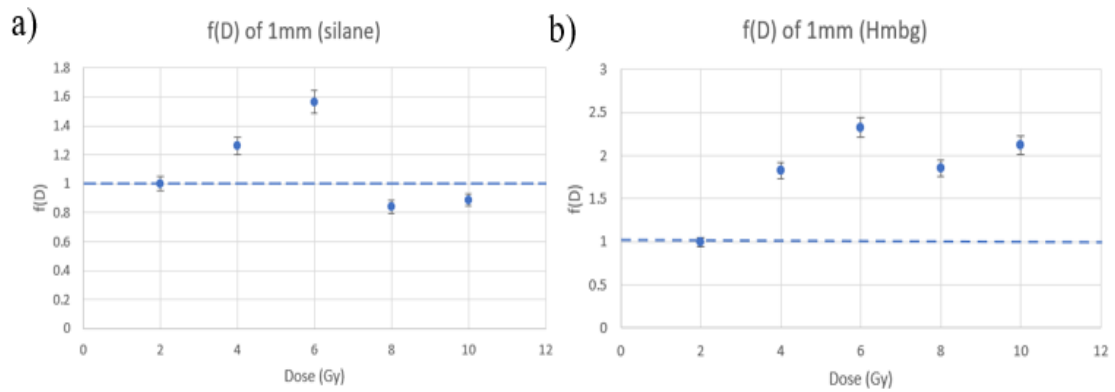
Figure 4.4 Linearity index of 1mm (Silane) and 1mm (Hmbg)

Table 4.3 Data required for the graph of 1mm (Silane) and 1mm (Hmbg)

Thickness,mm (Brand)	Dose (Gy)				
	2	4	6	8	10
f(D) of 1mm (Silane)	1	1.260893229	1.563079551	0.840601513	0.888997251
f(D) of 1mm (Hmbg)	1	1.824746655	2.327783797	1.856587202	2.11956866

4.2   Optical Characteristics

### 4.2.1   Fourier Transform Infrared (FTIR) spectra

Fourier transfer infrared spectroscopy (FTIR) was used to gather information on the infrared spectrum of adsorption, which corresponds to the frequency of vibration between the atomic bonds of the material. This information may be obtained by examining the adsorption spectrum. The intensity of the FTIR peak reveals the sample's constituents in a clear manner. Figure 4.5 illustrates, for the wavenumber range of 500 to 4000 cm^{-1}, quantitative information on the change in structure of the microscope glass slide produced by irradiation, as well as the difference between the spectra of irradiated and unirradiated samples. In order to do a qualitative study, the spectrum is divided into three regions. These areas consist of: 500-1,400 cm^{-1} (at fingerprint region), 1,400-2000 cm^{-1}, and 2000-2,500 cm^{-1} (refer Figure 4.6). The FTIR spectrum of the Si–O stretching region of the microscope glass slide is visible in the 1060 cm^{-1} band, as shown in Figure 4.5. However, owing to the stretching vibrations of the BO_4 tetrahedron, the boron structure may be seen at roughly 1000 cm^{-1} (Osipov et al., 2019; Peuget et al., 2013; Su & Suarez, 1995; Wan et al., 2008).The FTIR band of the microscope glass slide, which can be found between 800 and 1270 cm^{-1} and is centred at 1000 cm^{-1} (Elbatal et al., 2016) is a combination of the stretching vibration of the Si-O-Si network of tetrahedral structural units and the B-O-B network. This was able to be discovered in the fingerprint area, as shown in Figure 4.6. These components consist of groups like borate and silicate (Dalby & King, 2006; Du & Stebbin et al., 2016; El-Damrawi et al., 2016; Elbatal et al., 2016; Nesbitt & Bancroft, 2014).

According to (Stoch & Środa, 1999), the emergence of a small peak at around 700 cm-1 is generated by the bending vibrations of bridging oxygen between trigonal boron atoms. This was found in their analysis of the spectral data. After being subjected to gamma radiation, there is no change to the location of the FTIR band that spans between 800 and

1000 cm^{-1}. This is consistent with the primary composition of the microscope slide, which is made up of tetrahedral units of borate and silicate groups. This process affects the degree to which the glass-forming network is connected to one another and makes a substantial contribution to the radiation resistance of glass. The second discovery indicates that microscope glass slides are ideal for use in dosimetry sterilisation applications, as shown by the thermoluminescence study of (Ismail, et al., 2020). The most striking consequence of gamma irradiation is a dramatic decrease in frequency in the 800 cm^{-1} band, followed by an increase in frequency around 1000 cm^{-1}. The band detected between 1500 and 1700 cm^{-1} is a result of the vibration of water molecules (Baccaro et al., 2007; Qian et al., 2007)

For X-ray ,the general spectra for 1mm (silane) and 1mm (Hmbg) is quite similar but the peak for 1mm (silane) at 2165 to 2350 cm^{-1}.This shows that the functional group or network stretching found at the aforementioned wavenumber is more concentrated for 1mm (Silane) compared to 1mm (Hmbg). The network stretching that is present in this ranges is C≡C stretching at 2100 to 2250 cm^{-1} (alkyne group) as tabulated in Table 4.4 (Böhnke et al., 2015; Gouget-Laemmel et al., 2013). This is due to the inhomogeneity present in the sample of borosilicate (Alqahtani et al., 2020; Nazeri et al., 2021; Sani, Othman, et al., 2020a; Wan et al., 2008).
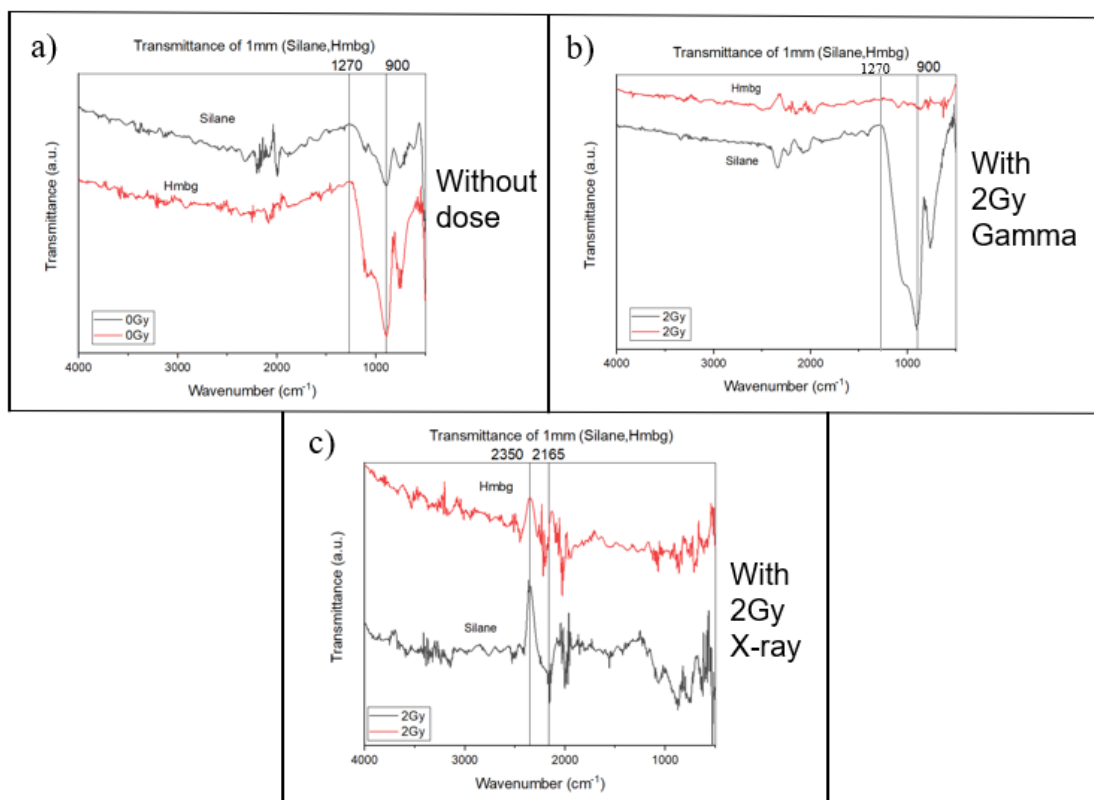
Figure 4.5 FTIR band of 1mm (Silane) fitted with 1mm (Hmbg) of unirradiated and irradiated with Photon (gamma and x-ray) (at 2 Gy).
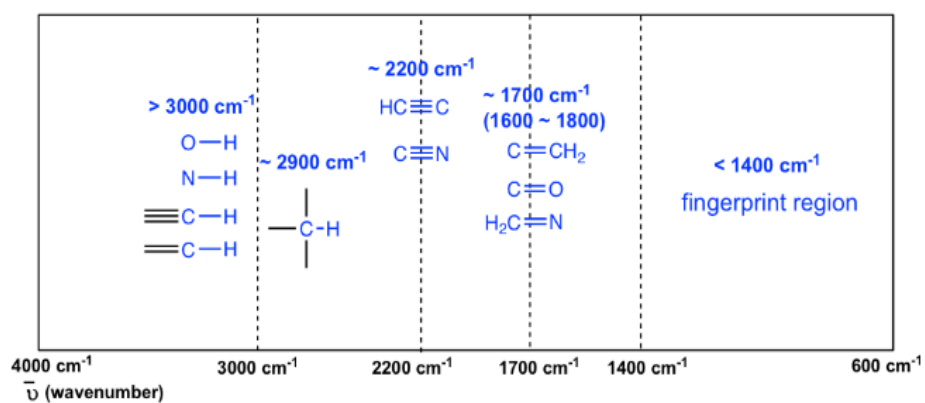

Figure 4.6 IR absorption Range

Table 4.4 Characteristic IR Frequencies of Stretching Vibrations

Formula	Bond	Characteristic IR Frequency Range, cm^{-1}
Alcohol	O-H stretching	3200-3600 (broad)
Carbonyl	C=O stretching	1650-1750 (strong)
Aldehyde	C-H stretching	~ 2800 and ~ 2700 (medium)
Carboxylic acid	C=O stretching	1700-1725 (strong)
Carboxylic acid	O-H stretching	2500-3300 (broad)
Alkene	C=C stretching	1620-1680 (weak)
Alkene	Vinyl = C-H stretching	3020-3080
Benzene	C=C stretching	~ 1600 and 1500-1430 (strong to weak)
Alkyne	C≡C stretching	2100-2250 (weak)
Alkyne	terminal≡C-H stretching	3250-3350
Alkane	C-H stretching	2850-2950
Amine	N-H stretching	3300-3500 (medium)

4.2.2 Raman spectra

Due to its great sensitivity to the existence of structural defects and relative non-destructiveness, Raman spectroscopy has become an established tool for assessing radiation damage on materials. Figure 4.7 depicts the room-temperature Raman spectra of a microscope glass slide treated with 0 to 8 Gy of 60Co gamma rays. Using OriginPro 2018 software, the Raman peaks were fitted to represent the vibrational bands in the glass medium. Figure 4.7(a) depicts the prominent peaks of a microscope glass slide at 595, 796, and 1091 cm^{-1} Raman bands for 0 and 2 Gy doses, whereas Figure 4.7(b) depicts the peaks at 609, 693, and 810 cm^{-1} Raman bands for 4, 6, and 8 Gy doses. It was found that the Raman band at 595 cm^{-1} is characteristic of ring breathing modes for the microscope glass slide that was studied. Furthermore, subsequent deconvolution of the spectra led to the identification of metaborate rings as well as other borate- and borosilicate-ring unit groups. The Raman peak that can be seen beneath the band at 550 cm^{-1} is the result of pair vibrations of the same sort that were brought about by a shift in the Si-O-Si angle. This shift brought about an asymmetric band. The breathing mode of borosilicate rings, which displays its features in the region of 550 to 850 cm^{-1}, is correlated to the 609 cm^{-1} and 693 cm^{-1} Raman bands (Meera et al., 1990; Meera & Ramakrishna, 1993).The prominent Raman band at 796 cm^{-1} is attributed to the bending vibration of the B-O-B bond thus possessing the behaviour of boroxol ring and four-coordinated boron in diborate (Iliescu et al., 1993; Konijnendijk & Stevels, 1975, 1976; Maniu et al., 1997; Meera et al., 1990).The region of frequency that corresponds to the 810 cm^{-1} Raman band is consistent with the stretching and deformation modes of the Si-O-Si bond. The Si-O-stretching in a structural unit with one oxygen atom for every silicon atom that does not bridge is responsible for the strong band that has a frequency of roughly 1091 cm^{-1}. It is believed that the aforementioned band corresponds to a vibrational frequency that is ascribed to a Si-O bridging oxygen stretching mode (Frantza & Mysen, 1995; McMillan

et al., 1994; Mysen & Frantz, 1994). Alternatively, it may correlate to a vibration in structural units that are coupled with the metal cation (Fukumi, Chayahara, et al., 1990; Fukumi, Hayakawa, et al., 1990; Neuville, 2006).
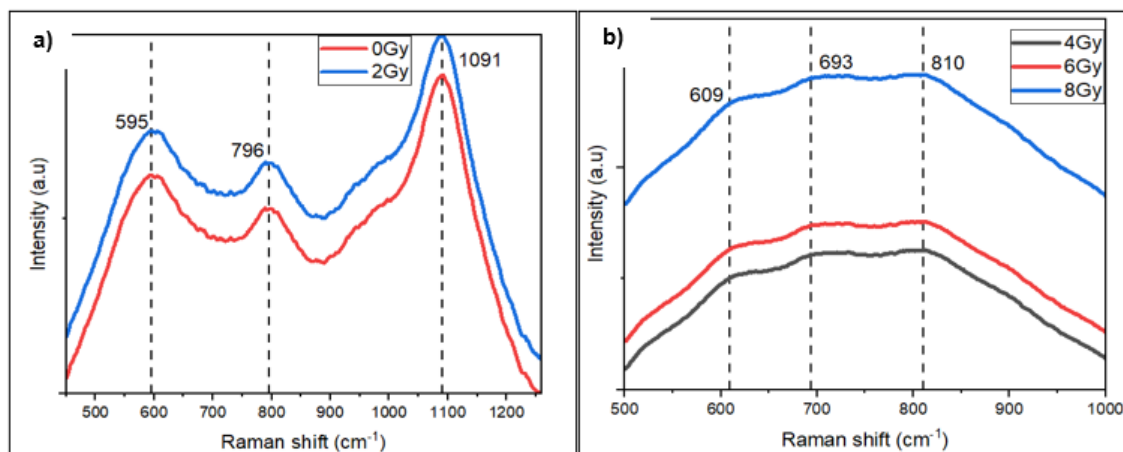
Figure 4.7 Raman Spectra of borosilicate glass slide subjected to 0 to 8 Gy of 60Co gamma rays.

CHAPTER 5: CONCLUSION

5.1 Conclusion

The thermoluminescence properties of 1mm thickness of borosilicate glass irradiated by Neutron source have been characterized. The optical characteristics of borosilicate glass slide by using the FTIR and Raman spectroscopy when exposed to photon (gamma and x-rays) irradiation have been determined. According to the findings of the current study, borosilicate glass has the appropriate qualities to make an improvement in radiation dosimetry, which is in accordance with the findings of previous research. The dose response graph demonstrates that 1mm (Hmbg) is a more appropriate material for use in medical dosimetry than 1mm (silane). In the field of medical dosimetry, it is essential to have linearity that fluctuates by no more than 1 standard deviation (3 %). It is acceptable for use as a medical dosimeter since the dosage response of 1mm (Hmbg) has a dose response linearity of less than 3 %, which validates the assertion made in the previous paragraph.

5.2 Future work

In the current study, it was determined that 1mm (Hmbg) had a variety of useful thermoluminescence features. Thus, future work on its application is essential to establish borosilicate glass as an alternative TL dosimeter for prospective usage in medical treatment applications. This is because it would be advantageous to do a thorough analysis of borosilicate glass so that it may be applied to patients.

REFERENCES

Alawiah & Hairul. (2015). *The thermoluminescence glow curve and the deconvoluted glow peak characteristics of Erbium doped silica fiber exposed to 70-130 kVp x-rays*. https://www.academia.edu/14435462/The_thermoluminescence_glow_curve_and_ the_deconvoluted_glow_peak_characteristics_of_Erbium_doped_silica_fiber_expo sed_to_70_130_kVp_x_rays

Alawiah, A., Bauk, S., Abdul-Rashid, H. A., Gieszczyk, W., Hashim, S., Mahdiraji, G. A., Tamchek, N., & Bradley, D. A. (2015). Potential application of pure silica optical flat fibers for radiation therapy dosimetry. *Radiation Physics and Chemistry*, *106*, 73–76. https://doi.org/10.1016/J.RADPHYSCHEM.2014.06.006

Alqahtani, A., Bradley, D. A., Alanizi, A., & Nisbet, A. (2020). Characterisation of borosilicate glass media as potential thermoluminescent dosimeters. *Radiation Physics and Chemistry*, *168*, 108630. https://doi.org/10.1016/J.RADPHYSCHEM.2019.108630

Baccaro, S., Monika, Sharma, G., Thind, K. S., Singh, D., & Cecillia, A. (2007). Analysis of structural modifications in γ-irradiated PbO–B2O3–SiO2 glasses by FTIR spectroscopy. *Nuclear Instruments and Methods in Physics Research Section B: Beam Interactions with Materials and Atoms*, *260*(2), 613–618. https://doi.org/10.1016/J.NIMB.2007.04.214

Boffy, R., Peuget, S., Schweins, R., Beaucour, J., & Bermejo, F. J. (2016). High thermal neutron flux effects on structural and macroscopic properties of alkali-borosilicate glasses used as neutron guide substrate. *Nuclear Instruments and Methods in Physics Research Section B: Beam Interactions with Materials and Atoms*, *374*, 14–19.

https://doi.org/10.1016/J.NIMB.2015.10.011

Böhnke, J., Braunschweig, H., Constantinidis, P., Dellermann, T., Ewing, W. C., Fischer, I., Hammond, K., Hupp, F., Mies, J., Schmitt, H. C., & Vargas, A. (2015). Experimental assessment of the strengths of B-B triple bonds. *Journal of the American Chemical Society*, *137*(5), 1766–1769. https://doi.org/10.1021/JA5116293/SUPPL_FILE/JA5116293_SI_002.CIF

Bradley, D. A., Nawi, S. N. M., Khandaker, M. U., Almugren, K. S., & Sani, S. F. A. (2020). Sub kGy photon irradiation alterations in graphite. *Applied Radiation and Isotopes*, *161*, 109168. https://doi.org/10.1016/J.APRADISO.2020.109168

Brundha, M. P., Pathmashri, V. P., & Sundari, S. (2019). Quantitative changes of red blood cells in cancer patients under palliative radiotherapy-a retrospective study. *Research Journal of Pharmacy and Technology*, *12*(2), 687–692. https://doi.org/10.5958/0974-360X.2019.00122.7

Bull, R. K. (1986). Thermoluminescence and its applications: an introduction. *International Journal of Radiation Applications and Instrumentation. Part D. Nuclear Tracks and Radiation Measurements*, *11*(1–2), 105–113. https://doi.org/10.1016/1359-0189(86)90029-4

Chen, C., Lin, H., Zhou, S., Zhang, S., Yi, X., Tang, Y., & Feng, Y. (2015). Composite phase ceramic phosphor of Al_2O_3-Ce:YAG for high efficiency light emitting. *Optics Express, Vol. 23, Issue 14, Pp. 17923-17928*, *23*(14), 17923–17928. https://doi.org/10.1364/OE.23.017923

Chen, R., & McKeever, S. W. S. (1997). Theory of Thermoluminescence and Related Phenomena. *Theory of Thermoluminescence and Related Phenomena*.

https://doi.org/10.1142/2781

Dalby, K. N., & King, P. L. (2006). A new approach to determine and quantify structural units in silicate glasses using micro-reflectance Fourier-Transform infrared spectroscopy. *American Mineralogist*, *91*(11–12), 1783–1793. https://doi.org/10.2138/AM.2006.2075

Daniels, F., Boyd, C. A., & Saunders, D. F. (1953). Thermoluminescence as a research tool. *Science*, *117*(3040), 343–349. https://doi.org/10.1126/SCIENCE.117.3040.343/ASSET/0DA89F8B-97A7-4C06-8BEA-1CD3543B2143/ASSETS/SCIENCE.117.3040.343.FP.PNG

DeWerd, L. A., & Stoebe, T. G. (1972). The emission spectrum of LiF (TLD-100) at low and high exposures. *Physics in Medicine & Biology*, *17*(2), 187. https://doi.org/10.1088/0031-9155/17/2/003

Du & Stebbin, Li, Z., Sun, Y., Liu, L., & Zhang, Z. (2016). Modification of the Structure of Ti-Bearing Mold Flux by the Simultaneous Addition of B2O3 and Na2O. *Metallurgical and Materials Transactions E 2016 3:1*, *3*(1), 28–36. https://doi.org/10.1007/S40553-016-0066-0

El-Damrawi, G., Hassan, A. M., Ramadan, R., & El-Jadal, S. (2016). Nuclear Magnetic Resonance and FTIR Structural Studies on Borosilicate Glasses Containing Iron Oxide. *New Journal of Glass and Ceramics*, *06*(04), 47–56. https://doi.org/10.4236/NJGC.2016.64006

Elbatal, H. A., Abdelghany, A. M., Ouis, M. A., Azooz, M. A., & El-Bassyouni, G. T. (2016). Role of SrO on the bioactivity behavior of some ternary borate glasses and their glass ceramic derivatives. *Spectrochimica Acta Part A: Molecular and*

Biomolecular Spectroscopy, *152*, 126–133. https://doi.org/10.1016/J.SAA.2015.07.072

Fadzil, Hassan, M. F., Abdul Rahman, W. N. W., Tominaga, T., Geso, M., Akasaka, H., Bradley, D. A., & Noor, N. M. (2017). The thermoluminescence response of Ge-doped flat fibre for proton beam measurements: A preliminary study. *Journal of Physics: Conference Series*, *851*(1), 012034. https://doi.org/10.1088/1742-6596/851/1/012034

Frantza, J. D., & Mysen, B. O. (1995). Raman spectra and structure of BaO☐SiO2 SrO☐SiO2 and CaO☐SiO2 melts to 1600°C. *Chemical Geology*, *121*(1–4), 155–176. https://doi.org/10.1016/0009-2541(94)00127-T

Fukumi, K., Chayahara, A., Satou, M., Hayakawa, J., Hangyo, M., & Nakashima, S. ichi. (1990). Surface structure of ion-implanted silica glass. *Japanese Journal of Applied Physics*, *29*(5 R), 905–908. https://doi.org/10.1143/JJAP.29.905/XML

Fukumi, K., Hayakawa, J., & Komiyama, T. (1990). Intensity of raman band in silicate glasses. *Journal of Non-Crystalline Solids*, *119*(3), 297–302. https://doi.org/10.1016/0022-3093(90)90302-3

Furetta, C. (2003). Handbook of Thermoluminescence. *Handbook of Thermoluminescence*. https://doi.org/10.1142/5167

Gouget-Laemmel, A. C., Yang, J., Lodhi, M. A., Siriwardena, A., Aureau, D., Boukherroub, R., Chazalviel, J. N., Ozanam, F., & Szunerits, S. (2013). Functionalization of azide-terminated silicon surfaces with glycans using click chemistry: XPS and FTIR study. *Journal of Physical Chemistry C*, *117*(1), 368–375. https://doi.org/10.1021/JP309866D/SUPPL_FILE/JP309866D_SI_001.PDF

Griffiths, P. R., & De Haseth, J. A. (2006). Fourier Transform Infrared Spectrometry: Second Edition. *Fourier Transform Infrared Spectrometry: Second Edition*, 1–529. https://doi.org/10.1002/047010631X

Hanna, D. W. (n.d.). *ANALYZER SYSTEM FOR LOW-DOSE MEASUREMENTS UTILIZING PHOTON COUNTING TECHNIQUES*.

Harvey, E. N. (2011). A history of luminescence from the earliest times until 1900. *A History of Luminescence from the Earliest Times until 1900*. https://doi.org/10.5962/BHL.TITLE.14249

Hashim, S., Bradley, D. A., Peng, N., Ramli, A. T., & Wagiran, H. (2010). The thermoluminescence response of oxygen-doped optical fibres subjected to photon and electron irradiations. *Nuclear Instruments and Methods in Physics Research Section A: Accelerators, Spectrometers, Detectors and Associated Equipment*, *619*(1–3), 291–294. https://doi.org/10.1016/J.NIMA.2009.10.109

Hashim, S., Omar, S. S. C., Ibrahim, S. A., Hassan, W. M. S. W., Ung, N. M., Mahdiraji, G. A., Bradley, D. A., & Alzimami, K. (2015). Thermoluminescence response of flat optical fiber subjected to 9 MeV electron irradiations. *Radiation Physics and Chemistry*, *106*, 46–49. https://doi.org/10.1016/J.RADPHYSCHEM.2014.06.028

Huston, A. L., Justus, B. L., Falkenstein, P. L., Miller, R. W., Ning, H., & Altemus, R. (2001). Remote optical fiber dosimetry. *Nuclear Instruments and Methods in Physics Research Section B: Beam Interactions with Materials and Atoms*, *184*(1–2), 55–67. https://doi.org/10.1016/S0168-583X(01)00713-3

Ibrahim, A., Férachou, D., Sharma, G., Singh, K., Kirouac-Turmel, M., & Ozaki, T. (2016). Ultra-high dynamic range electro-optic sampling for detecting millimeter

and sub-millimeter radiation. *Scientific Reports 2016 6:1*, *6*(1), 1–9. https://doi.org/10.1038/srep23107

Iliescu, T., Simon, S., Maniu, D., & Ardelean, I. (1993). Raman spectroscopy of oxide glass system (1-x) [yB2O3.zLi2O].xGd2O3. *Journal of Molecular Structure*, *294*(C), 201–203. https://doi.org/10.1016/0022-2860(93)80349-Z

Izewska, J., & Andreo, P. (2000). The IAEA/WHO TLD postal programme for radiotherapy hospitals. *Radiotherapy and Oncology : Journal of the European Society for Therapeutic Radiology and Oncology*, *54*(1), 65–72. https://doi.org/10.1016/S0167-8140(99)00164-4

Kinchin, G. H., & Pease, R. S. (1955). The Displacement of Atoms in Solids by Radiation. *Reports on Progress in Physics*, *18*(1), 1. https://doi.org/10.1088/0034-4885/18/1/301

Konijnendijk, W. L., & Stevels, J. M. (1975). The structure of borate glasses studied by Raman scattering. *Journal of Non-Crystalline Solids*, *18*(3), 307–331. https://doi.org/10.1016/0022-3093(75)90137-4

Konijnendijk, W. L., & Stevels, J. M. (1976). The structure of borosilicate glasses studied by Raman scattering. *Journal of Non-Crystalline Solids*, *20*(2), 193–224. https://doi.org/10.1016/0022-3093(76)90132-0

Kozima, H. (2006). The Science of the Cold Fusion Phenomenon. *The Science of the Cold Fusion Phenomenon*, 67–114. https://doi.org/10.1016/B978-008045110-7/50004-6

Kraevskii, S. L. (2001). An Alternative Model for Photochromism of Glasses: Reversible Injection of Carriers from a Microcrystal and Its Surface States into Point Defects of Glass. *Glass Physics and Chemistry 2001 27:4*, *27*(4), 315–330.

https://doi.org/10.1023/A:1011312109403

Kron, Liuzzi, R., Piccolo, C., D'Avino, V., Clemente, S., Oliviero, C., Cella, L., & Pugliese, M. (1999). Dose-Response of TLD-100 in the Dose Range Useful for Hypofractionated Radiotherapy. *Dose-Response : A Publication of International Hormesis Society*, *18*(1), 1559325819894081. https://doi.org/10.1177/1559325819894081

Kumar, D., Bhatia, V., Rao, S. M., Chen, C. L., Kaur, N., & Singh, S. P. (2020). Synthesis of NaSrB:Nd3+ glass system for the analysis of structural, optical and thermoluminescence properties. *Materials Chemistry and Physics*, *243*. https://doi.org/10.1016/J.MATCHEMPHYS.2019.122546

Maniu, D., Ardelean, I., Iliescu, T., Cinta, S., & Cozar, O. (1997). Raman spectroscopic investigations of the oxide glass system $(1 - x)(3B2O3 \cdot K2O)xMO$ (MO = V2O5 or CuO). *Journal of Molecular Structure*, *410–411*, 291–294. https://doi.org/10.1016/S0022-2860(96)09674-3

Mayerhöfer, T. G., Pahlow, S., & Popp, J. (2020). The Bouguer-Beer-Lambert Law: Shining Light on the Obscure. *ChemPhysChem*, *21*(18), 2029–2046. https://doi.org/10.1002/CPHC.202000464

McKeever, S. W. S., Moscovitch, M., & Townsend, P. D. (Peter D. (1995). *Thermoluminescence dosimetry materials : properties and uses*. Nuclear Technology Pub.,.

McKinley. (1981). *The optimization and use of a photon counting system for thermoluminescent dosimetry*. https://iopscience.iop.org/chapter/978-0-7503-1317-9/bk978-0-7503-1317-9ch1.pdf

McMillan, P. F., Poe, B. T., Gillet, P. H., & Reynard, B. (1994). A study of SiO2 glass and supercooled liquid to 1950 K via high-temperature Raman spectroscopy. *Geochimica et Cosmochimica Acta*, *58*(17), 3653–3664. https://doi.org/10.1016/0016-7037(94)90156-2

Meera, B. N., & Ramakrishna, J. (1993). Raman spectral studies of borate glasses. *Journal of Non-Crystalline Solids*, *159*(1–2), 1–21. https://doi.org/10.1016/0022-3093(93)91277-A

Meera, B. N., Sood, A. K., Chandrabhas, N., & Ramakrishna, J. (1990). Raman study of lead borate glasses. *Journal of Non-Crystalline Solids*, *126*(3), 224–230. https://doi.org/10.1016/0022-3093(90)90823-5

Mysen, B. O., & Frantz, J. D. (1994). Silicate melts at magmatic temperatures: in-situ structure determination to 1651°C and effect of temperature and bulk composition on the mixing behavior of structural units. *Contributions to Mineralogy and Petrology 1994 117:1*, *117*(1), 1–14. https://doi.org/10.1007/BF00307725

Nabil El Faramawy. (n.d.). *(1) (PDF) Current Research Paper Dosimetric properties of in-house prepared MgB 4 O 7 :Dy*. Retrieved June 18, 2022, from https://www.researchgate.net/publication/350214729_Current_Research_Paper_Dosimetric_properties_of_in-house_prepared_MgB_4_O_7_Dy

Nazeri, A. A. Z. A., Sani, S. F. A., Ung, N. M., Almugren, K. S., Alkallas, F. H., & Bradley, D. A. (2021). Borosilicate glass 60Co high dose rate brachytherapy thermoluminescence dosimetry. *Applied Radiation and Isotopes*, *176*, 109814. https://doi.org/10.1016/J.APRADISO.2021.109814

Nesbitt, H. W., & Bancroft, G. M. (2014). High Resolution Core- and Valence-Level XPS

Studies of the Properties (Structural, Chemical and Bonding) of Silicate Minerals and Glasses. *Reviews in Mineralogy and Geochemistry*, *78*(1), 271–329. https://doi.org/10.2138/RMG.2014.78.7

Neuville, D. R. (2006). Viscosity, structure and mixing in (Ca, Na) silicate melts. *Chemical Geology*, *229*(1–3), 28–41. https://doi.org/10.1016/J.CHEMGEO.2006.01.008

Osipov, A. A., Osipova, L. M., Hruška, B., Osipov, A. A., & Liška, M. (2019). FTIR and Raman spectroscopy studies of ZnO-doped BaO·2B2O3 glass matrix. *Vibrational Spectroscopy*, *103*, 102921. https://doi.org/10.1016/J.VIBSPEC.2019.05.003

Patra, G. D., Singh, S. G., Tiwari, B., Singh, A. K., Desai, D. G., Tyagi, M., Sen, S., & Gadkari, S. C. (2016). Optically stimulated luminescence in Ag doped Li2B4O7 single crystal and its sensitivity to neutron detection and dosimetry in OSL mode. *Radiation Measurements*, *88*, 14–19. https://doi.org/10.1016/J.RADMEAS.2016.03.002

Peuget, S., Maugeri, E. A., Charpentier, T., Mendoza, C., Moskura, M., Fares, T., Bouty, O., & Jégou, C. (2013). Comparison of radiation and quenching rate effects on the structure of a sodium borosilicate glass. *Journal of Non-Crystalline Solids*, *378*, 201–212. https://doi.org/10.1016/J.JNONCRYSOL.2013.07.019

Pynn, R. (2009). *Neutron Scattering—A Non-destructive Microscope for Seeing Inside Matter*. 15–36. https://doi.org/10.1007/978-0-387-09416-8_2

Qian, G., Baccaro, S., Guerra, A., Xiaoluan, L., Shuanglong, Y., Iurlaro, G., & Chen, G. (2007). Gamma irradiation effects on ZnO-based scintillating glasses containing CeO2 and/or TiO2. *Nuclear Instruments and Methods in Physics Research Section*

B: Beam Interactions with Materials and Atoms, *262*(2), 276–280. https://doi.org/10.1016/J.NIMB.2007.06.005

Ranogajec-Komor, M. (2004). Thermoluminescence Personal and Medical Dosimetry. *Radiation Safety Problems in the Caspian Region*, 177–190. https://doi.org/10.1007/1-4020-2378-2_29

Rivera-Montalvo, T. (2014). Radiation therapy dosimetry system. *Applied Radiation and Isotopes*, *83*, 204–209. https://doi.org/10.1016/J.APRADISO.2013.07.011

Rivera, T. (2012a). Thermoluminescence in medical dosimetry. *Applied Radiation and Isotopes*, *71*(SUPPL.), 30–34. https://doi.org/10.1016/J.APRADISO.2012.04.018

Rivera, T. (2012b). Thermoluminescence in medical dosimetry. *Applied Radiation and Isotopes*, *71*(SUPPL.), 30–34. https://doi.org/10.1016/J.APRADISO.2012.04.018

Saeed, M. A., Saidu, A., Wagiran, H., Saeed, M. A., Obayes, H. K., Bala, A., & Usman, F. (2018). Thermoluminescence response of rare earth activated zinc lithium borate glass. *Radiation Physics and Chemistry*, *144*, 413–418. https://doi.org/10.1016/J.RADPHYSCHEM.2017.10.004

Sani, S. F. A., Ismail, S. S., Almugren, K. S., Khandaker, M. U., & Bradley, D. A. (2020). Dosimetric utility of structural changes in gamma irradiated graphite-rich pencils. *Radiation Physics and Chemistry*, *171*, 108703. https://doi.org/10.1016/J.RADPHYSCHEM.2020.108703

Sani, S. F. A., Othman, M. H. U., Alqahtani, A., Almugren, K. S., Alkallas, F. H., & Bradley, D. A. (2020a). Low-cost commercial borosilicate glass slides for passive radiation dosimetry. *PLOS ONE*, *15*(12), e0241550. https://doi.org/10.1371/JOURNAL.PONE.0241550

Sani, S. F. A., Othman, M. H. U., Alqahtani, A., Almugren, K. S., Alkallas, F. H., & Bradley, D. A. (2020b). Low-cost commercial borosilicate glass slides for passive radiation dosimetry. *PLoS ONE*, *15*(12 December), e0241550. https://doi.org/10.1371/journal.pone.0241550

Sani, S. F. A., Othman, M. H. U., Alqahtani, A., Nazeri, A. A. Z. A., Almugren, K. S., Ung, N. M., Hashim, S. A., Alkallas, F. H., & Bradley, D. A. (2021). Passive dosimetry of electron irradiated borosilicate glass slides. *Radiation Physics and Chemistry*, *178*. https://doi.org/10.1016/j.radphyschem.2020.108903

Smedskjaer, M. M., Mauro, J. C., Youngman, R. E., Hogue, C. L., Potuzak, M., & Yue, Y. (2011). Topological principles of borosilicate glass chemistry. *Journal of Physical Chemistry B*, *115*(44), 12930–12946. https://doi.org/10.1021/JP208796B/ASSET/IMAGES/MEDIUM/JP-2011-08796B_0006.GIF

Stoch, L., & Środa, M. (1999). Infrared spectroscopy in the investigation of oxide glasses structure. *Journal of Molecular Structure*, *511–512*, 77–84. https://doi.org/10.1016/S0022-2860(99)00146-5

Su, C., & Suarez, D. L. (1995). Coordination of Msottod Boron: A FTIB Spectroscopic Study. *Environmental Science and Technology*, *29*(2), 302–311. https://doi.org/10.1021/ES00002A005/ASSET/ES00002A005.FP.PNG_V03

Suliman, I. I. (2007). *Patient Dosimetry and Quality Control in Diagnostic Radiology* . Medical Physics. https://inis.iaea.org/search/search.aspx?orig_q=RN:38096987

Townsend, P. D. (1990). *Thermoluminescence in solids and its applications*. International Journal of Radiation Applications and Instrumentation. Part D. Nuclear Tracks and

Radiation Measurements. https://doi.org/10.1016/1359-0189(90)90026-t

Vance, D. W. (2003). Surface Charging of Insulators by Ion Irradiation. *Journal of Applied Physics*, *42*(13), 5430. https://doi.org/10.1063/1.1659961

Wan, J., Cheng, J., & Lu, P. (2008). The coordination state of B and Al of borosilicate glass by IR spectra. *Journal of Wuhan University of Technology-Mater. Sci. Ed. 2008 23:3*, *23*(3), 419–421. https://doi.org/10.1007/S11595-007-3419-9

Xu, L., Chen, H., Zhang, X., -, al, Reinertsen, E., Clifford -, G. D., Ibrahim, S. A., Che Omar, S. S., Hashim, S., Mahdiraji, G. A., Bradley, D. A., Kadir, A. B., & Isa, N. M. (2014). Assessment of Ge-doped optical fibres subjected to x-ray irradiation. *Journal of Physics: Conference Series*, *546*(1), 012017. https://doi.org/10.1088/1742-6596/546/1/012017

Yaakob, N. H., Wagiran, H., Hossain, I., Ramli, A. T., Bradley, D. A., Hashim, S., & Ali, H. (2011). Electron irradiation response on Ge and Al-doped SiO2 optical fibres. *Nuclear Instruments and Methods in Physics Research Section A: Accelerators, Spectrometers, Detectors and Associated Equipment*, *637*(1), 185–189. https://doi.org/10.1016/J.NIMA.2011.02.041

Ying, L. T., Wagiran, H., Hashim, S., & Hussin, R. (2012). Overview of the Sensitivity of Ge- and Al-doped Silicon Dioxide Optical Fibres to Ionizing Radiation. *Malaysian Journal of Fundamental and Applied Sciences*, *8*(4), 270–274. https://doi.org/10.11113/MJFAS.V8N4.164

Zubair, H. T., Alqahtani, A., Sani, S. F. A., Abdul-Rashid, H. A., & Bradley, D. A. (2021). Development of borosilicate optical fibres for particle ionizing radiation dosimetry. *Optical Fiber Technology and Applications*. https://doi.org/10.1088/978-0-7503-

3243-9CH4